J. Chem. Sci. Vol. 129, No. 8, August 2017, pp. 1171–1181.
DOI 10.1007/s12039-017-1330-2

REGULAR ARTICLE

Carboxylate-bridged Cu(II) coordination polymeric complex: synthesis, crystal structure, magnetic properties, DNA binding and electrochemical studies

SABITHAKALA THATITURI[a], BHARGAVI GOVINDUGARI[b] and VENKATA RAMANA REDDY CHITTIREDDY[a,*]

[a]Department of Chemistry, Jawaharlal Nehru Technological University Hyderabad, Hyderabad, Telangana 500 085, India
[b]School of Chemistry, University of Hyderabad, Hyderabad, Telangana 500 046, India
E-mail: vrr9@yahoo.com

MS received 12 November 2016; revised 11 May 2017; accepted 18 May 2017

Abstract. A novel water-soluble carboxylate-bridged copper(II) coordination polymer, Cu-BIG was formed by the reaction of $Cu(ClO_4)_2 \cdot 6H_2O$ and tridentate benzimidazole-glycine conjugate ligand, 2-((1H-benzimidazol-2-yl)methylamino) acetic acid, BIGH and its structure has been determined by IR, UV, powder XRD, VSM, CV, TGA, DTA, EPR and single crystal X-ray diffraction. Crystallographic studies indicate it to be a coordination polymer with Pī Space group. The asymmetric unit of complex contains two Cu(II) ions with elongated square pyramid geometry. The axial positions of the Cu(II) atoms are occupied by the carbonyl oxygen of the carboxylate group with the bond distances $Cu(1)–O(5)_{axial}$, 2.28 Å, and $Cu(2)–O(2)_{axial}$, 2.26 Å. The two Cu(II) are connected through the carboxylic group present in BIGH, which provides electron mobilisation in the molecule and hence results in the soft ferromagnetic polymer. An *in vitro* antibacterial activity study of BIGH and Cu-BIG showed moderate activity against *Bacillus subtilis*. The DNA binding studies showed the interaction of Cu-BIG with CT-DNA.

Keywords. Copper(II)polymeric complex; ferromagnetism; electrochemical studies; crystal structure.

1. Introduction

The design and synthesis of metal–organic coordination polymers (MOCPs) is an emerging area in the field of advanced materials research in recent years.[1–4] The study of MOCPs is exciting due to their diverse structures, properties and compositions. Their easy customizability in addition to fascinating structural topologies has further drawn the attention of many researchers, for their potential application as advanced functional materials in the fields of catalysis, non-linear optics, medicine, *etc*.[5–9] Consequently, many efforts have been devoted to the study of transition metal–organic coordination polymers. Especially, the MOCPs based on the N-donor heterocycles have been widely used as luminescence materials, catalysts, electrical and magnetic materials.[10–13] In view of the interesting applications, the present work has been carried out to synthesize a copper(II) coordination polymer of benzimidazole-glycine conjugate ligand, 2-((1H-benzimidazol-2-yl)methylamino) acetic acid, (BIGH), $[\{Cu\ (BIG)\ (H_2O)\}_2]_n\ (ClO_4)_{2n} \cdot 3nH_2O$. The BIGH consists of benzimidazole ring and carboxylic acid in its side chain, which facilitates the formation of MOCPs.[14–18] Owing to its versatile coordination modes, the terminal carboxylate group acts as a bridge to construct coordination polymer. The flexible and free carboxylate terminal in BIGH is conformationally diverse to form a stable covalent bond with metal ion. The Cu-BIG coordination polymer is connected through carboxylate group, [Cu(1)–O–C–O–Cu(2)], which acts as a bridge for electron mobilization between two copper atoms which in turn makes a soft ferromagnetic material. The crystal structure, magnetic properties, antibacterial activity and DNA binding studies of Cu-BIG have been carried out. The electron transfer mechanism of copper(II) complex was investigated by cyclic voltammetry.

*For correspondence

Electronic supplementary material: The online version of this article (doi:10.1007/s12039-017-1330-2) contains supplementary material, which is available to authorized users.

2. Experimental

2.1 *Chemicals*

All the chemicals such as iminodiacetic acid, o-phenylenediamine and Copper(II) perchlorate hexahydrate were used as obtained from Aldrich. All other chemicals and solvents used for the synthesis were reagent grade.

2.2 *Instrumentation*

IR spectrum was recorded on a JASCO FT-IR 5300 spectrometer. Elemental analysis for C, H and N was done using a FLASH Ea 1112 SERIES CHNS analyzer. EPR spectrum was obtained using BRUKER Xenon EMX-ER073 spectrometer. X-ray powder diffractograms were recorded on a SMART Bruker D8 advance X-ray diffractometer using Cu-K_α λ-radiation (λ = 1.5406Å) at 40 kV and 30 mA. Magnetic moments were recorded on Lakeshore VSM 7410. Diffuse reflectance spectra were obtained using a Shimadzu UV-3100 PC Spectrophotometer. Cyclic voltammograms were recorded using Gamry-600 electrochemical analyzer and Fluorescence measurements were made using Perkin Elmer LS45 fluorescence spectrometer. Thermo gravimetric analysis was made using Exstrar TG DTA 6300.

2.3 *Synthesis of 2-((1H-benzimidazol-2-yl)methylamino)acetic acid (BIGH)*

Iminodiacetic acid (15.98 g, 120.0 mmol) was dissolved in 100 mL of 6N HCl, and *o*−phenylenediamine (3.25 g, 30.0 mmol) in 20 mL of 4N HCl was added dropwise. The reaction mass was refluxed at 100°C for about 16 h. To this solution, *o*-phenylenediamine (3.25 g, 30.0 mmol) in 20 mL of 4N HCl was added and the reaction was continued for 72 h. The final green solution was cooled to room temperature. Green coloured precipitate obtained was filtered (dimer), and the clear brown coloured filtrate was allowed for solvent evaporation up to a minimum volume. A white solid formed was separated and dissolved in 100 mL of water and neutralized with 2N NaOH; above synthesis was done based on literature procedure.[19] Formed precipitate was collected and leached with cold methanol (80 mL) and dried in the oven. Yield: 4.7 g (23 mmol, 42%). M.p. : 205–210°C; ^{1}H NMR (400 MHz, DMSO-d_6, 25°C): δ = 7.5 (multiplet, 2H, Ar-H), 7.15 (multiplet, 2H, Ar-H), 4.1 (singlet, 2H, CH_2), 3.3 (singlet, 2H, CH_2COO), as shown in Figure S3 (Supplementary Information). IR data (KBr, cm^{-1}): 3460 (N–H), 1643 (C=O), 1596 (C=C aromatic), 1268 (C–N). Anal. Calcd. (%) for (BIGH): C, 58.53; H, 5.40; N, 20.48. Found (%): C, 58.42; H, 5.45; N, 20.36 as shown in Figure S4 (Supplementary Information).

2.3a *Synthesis of copper(II) complex, Cu-BIG (**1**)*: Synthesis of $\left[\{Cu\,(BIG)\,(H_2\,O)\}_2\right]_n\,(ClO_4)_{2n}\cdot 3nH_2\,O$ was done as follows. BIGH (0.250 g, 1.12 mmol) was dissolved in 25 mL water, to which 5 mL aqueous solution of $Cu(ClO_4)_2\cdot 6H_2O$ (0.45 g, 1.12 mmol) was added slowly and stirred for 5 min. The resultant dark blue coloured solution was filtered and kept for crystallization in desiccator over H_2SO_4. Good quality blue coloured single crystals obtained were collected after seven days. Yield: 0.72 g (0.87 mmol, 72%). IR data (KBr, cm^{-1}): 3435 (bound water), 3249 (N–H), 3228 (Ar-H), 1615 (C=O), 1285 (C–N).

2.4 *X-ray crystal structure determination*

X-ray diffraction data were collected for Cu-BIG complex on a BRUKER-AXS SMART APEX CCD X-ray diffractometer, using graphite-monochromatic Mo K α radiation (=0.71073 Å). Data were reduced using SAINTPLUS[20] and a multi-scan absorption correction using SADABS[21] was performed. The structures were solved using SHELXS-97[22] and full matrix least-squares refinements against F^2 were carried out using SHELXL-97.[23] All ring hydrogen atoms were assigned on the basis of geometrical considerations and were allowed to ride upon the respective carbon atoms. All hydrogen atoms were assigned fixed U_{iso} values, equal to $1.2U_{eq}$ of the parent atom for ring and $1.5U_{eq}$ for methyl hydrogens. Crystallographic data and structure refinement parameters are presented in Table 1.

Table 1. Crystal data and structure refinement details for Cu-BIG.

Formula	$C_{20}H_{30}Cl_2Cu_2N_6O_{17}$
Formula weight	824.48
Crystal system	Triclinic
a(Å)	7.0044(8)
b(Å)	11.8269(13)
c(Å)	18.495(2)
α(°)	88.306(2)
β(°)	85.763(2)
γ(°)	84.972(2)
V (Å^3)	1521.7(3)
Space group	P $\bar{1}$
Z	2
T (K)	298(2)
ρ_{calcd}(g cm^{-3})	1.799
μ (mm^{-1})	1.661
θ Range (°)	1.10–28.26
$h/k/l$ indices	–9, 9/ –15, 15/ –24, 24
Reflections collected	17733
Unique reflection, R_{int}	7083, 0.0285
GooF	1.038
$R_1[I > 2\sigma(I)]$	0.0509
wR_2 [all data]	0.1329
$\Delta\rho_{max}$, $\Delta\rho_{min}$(e · Å^{-3})	1.069, –0.542

3. Results and Discussion

3.1 *Crystal structure of* $[Cu(BIG)(H_2O)_2]_n(ClO_4)_{2n} \cdot 3nH_2O$

The reaction of $Cu(ClO_4)_2 \cdot 6H_2O$ with the tridendate ligand, BIGH in 1:1 molar ratio in aqueous medium, upon crystallization yields blue coloured stable Cu(II) coordination polymeric complex (Scheme 1). Yield 75%. The ORTEP[24] view of the complex with the labeling of non-hydrogen atoms is shown in Figure 1. The complex, Cu-BIG crystallizes into the triclinic system with space group $P\bar{1}$. The asymmetric unit of the complex contains two Cu(II) ions with elongated square pyramid geometry. Three of the basal coordination sites of Cu(II) ions are occupied by the secondary amino nitrogen (Cu(1)–N(1), 2.01 Å; Cu(2)–N(4), 2.02 Å), the imidazole nitrogen (Cu(1)–N(2), 1.96 Å; Cu(2)–N(4), 1.96 Å) and the carboxylate oxygen (Cu(1)–O(1), 1.96 Å; Cu(2)–O(4), 1.95 Å) of the ligand. The fourth position of the basal plane is occupied by neutral water molecule with the bond distance, Cu(1)–O(3W), 1.98 Å; Cu(2)–O(6W), 1.97 Å. The axial positions of the Cu(II) ions are occupied by the carbonyl oxygen of the carboxylate group with the bond distances $Cu(1)–O(5)_{axial}$, 2.28 Å; $Cu(2)–O(2)_{axial}$, 2.26 Å. The two Cu(II) ions are connected through the carboxyl oxygen atom of a carboxylic group and form a dimeric unit. Cu-BIG is freely soluble in an aqueous medium due to the deprotonated ligand is which involved in the polymer formation.

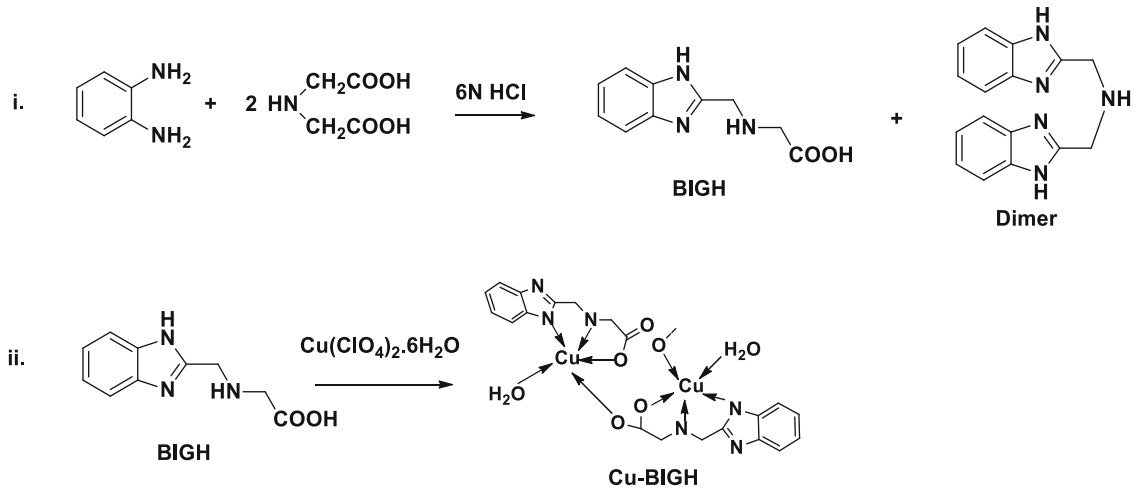

Scheme 1. Schematic representation of the synthesis of Cu-BIG complex.

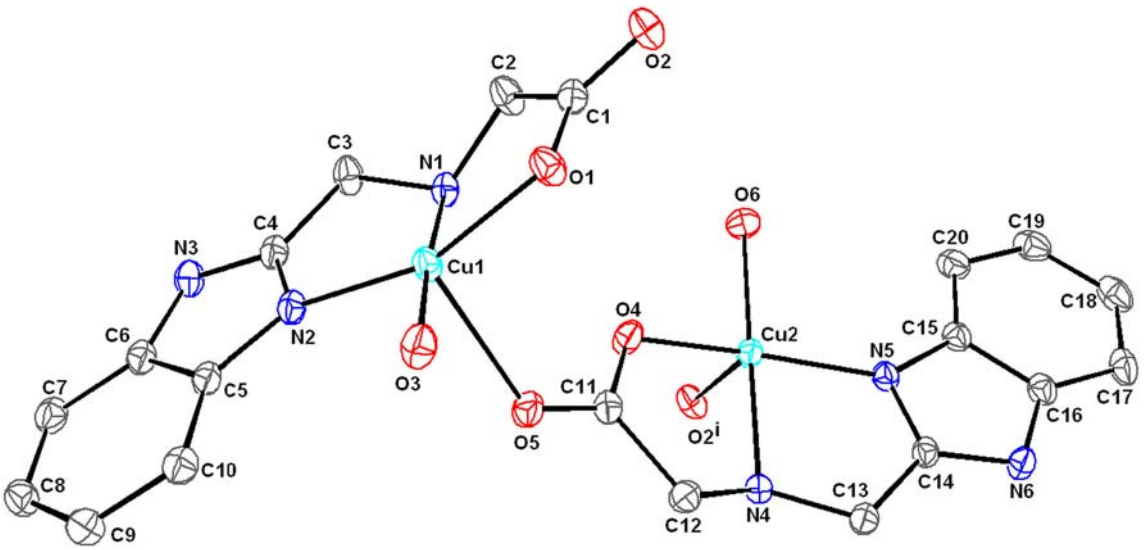

Figure 1. ORTEP view of the dimeric unit of $[\{Cu(BIG)(H_2O)\}_2]_n(ClO_4)_{2n} \cdot 3nH_2O$. Hydrogen atoms are omitted for the sake of clarity and the thermal ellipsoids are represented at the 30% probability level. Symmetry transformation [i = $x - 1$, y, z].

The dimeric units are translated along the crystallographic *a*-axis, leading to a polymeric zig-zag chain (Figure 2). Bond angles in the square plane vary from 83.0(1)° to 100.8(1)°. The metal ion lies 0.13 Å out of the least-squares basal plane, towards $O(5)_{axial}$. The axial Cu–O(5) bond is longer by 0.31 Å than the Cu–O bond lengths in the basal plane. The molecular geometry is close to that predicted for M(tridentate)(monodentate)$_2$ systems by simple donor atom repulsion theory.[25] Analysis data of bond length and bond angles are listed in Tables 2 and 3. Neighbouring copper ions in the polymer are linked through

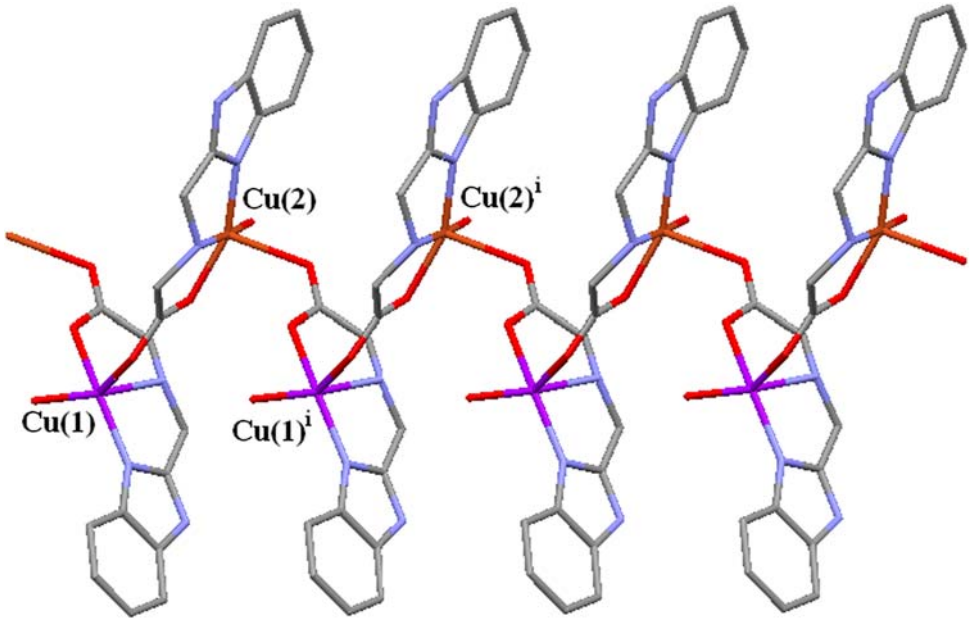

Figure 2. Perspective view of zig-zag polymeric chain of $[\{Cu(BIG)(H_2O)\}_2]_n(ClO_4)_{2n} \cdot 3nH_2O$ along the *a*-axis (i = $x-1,\ y,\ z$). *Colour* code for atoms: *grey* C; *blue* N; *red* O; *violet* Cu(1); brick *red* Cu(2).

Table 2. Selected bond lengths (Å) and angles (°) for Cu-BIG complex.

Bond	Bond length(Å)	Bond	Bond length(Å)	Bond	Bond length(Å)
Cu1–O1	1.962(2)	Cu2–O6	1.972(3)	Cl1–O7	1.438(3)
Cu1–O3	1.978(2)	Cu2–O4	1.949(2)	Cl1–O8	1.421(3)
Cu1–N1	2.011(3)	Cu2–N4	2.017(3)	Cl1–O9	1.362(5)
Cu1–N2	1.963(3)	Cu2–N5	1.954(3)	Cl1–O10	1.421(5)
Cu1–O5	2.281(2)	Cu2–O2#1	2.254(2)	Cl2–O11	1.438(5)
Cl2–O12	1.367(9)	Cl2–O13	1.333(4)	Cl2–O14	1.249(5)

Symmetry transformation = #1$x+1, y, z$ #2$x-1, y, z$.

Table 3. Selected bond angles (°) for Cu-BIG complex.

Angle	Bond angle (°)	Angle	Bond angle (°)	Angle	Bond angle (°)
O1–Cu1–N1	83.76(11)	O4–Cu2–N4	84.66(10)	O4–Cu2–O2#1	101.09(10)
O1–Cu1–N2	159.15(11)	O4–Cu2–06	93.80(11)	N4–Cu2–O2#1	96.44(10)
O1–Cu1–O3	92.85(11)	O4–Cu2–N5	157.51(11)	O6–Cu2–O2#1	87.32(11)
O1–Cu1–O5	98.41(10)	O6–Cu2–N4	176.14(12)	N5–Cu2–O2#1	98.81(10)
O3–Cu1–N1	176.08(11)	N1–Cu1–O5	96.86(10)	O4–Cu2–O2#2	55.68(8)
O3–Cu1–O5	81.67(10)	N5–Cu2–O6	97.50(11)	N5–Cu2–O2#2	112.20(8)
N2–Cu1–O3	100.79(11)	N5–Cu2–N4	82.80(11)	O6–Cu2–O2#2	65.74(9)
N2–Cu1–N1	83.01(11)	N4–Cu2–O2#2	110.56(8)		
N2–Cu1–O5	99.11(10)	O2#1–Cu2–O2#2	140.62(8)		

Symmetry transformation = #1$x+1, y, z$ #2$x-1, y, z$.

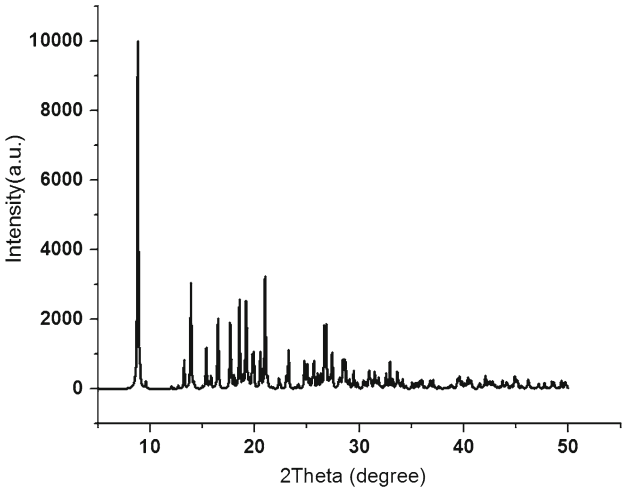

Figure 3. Powder X-ray diffraction patterns of Cu-BIG.

terminal carboxylate oxygen atoms of the ligand and form a ···Cu···O–C—O--Cu–O···Cu··· zigzag syn-anti conformational chain (Figure 3). The closest Cu ···Cu distance in this polymeric chain is 5.33 Å. The polymeric chain is additionally stabilized by the presence of hydrogen bonds involving the carboxylate oxygen, perchlorate and coordinated lattice water molecules.

3.2 *Infrared spectral analysis*

The IR spectrum of the BIGH shows several IR absorption frequencies appearing at 3462, 3013, and 2783 cm^{-1} due to N–H stretching of secondary amine in the side chain, N–H stretching imidazole ring and O–H stretching of carboxylic acid, respectively. These frequencies are absent in the IR spectrum of the complex Cu-BIG. Thus, it confirms the involvement of nitrogen and oxygen atom in chelation with metal ion. Hence, a broad band at 3400 cm^{-1} indicates the presence of a water molecule in the complex, as shown in Figures S1 and S2 (Supplementary Information).

3.3 *DNA binding studies*

Generally, the DNA shows hyperchromism or hypochromism when it reacts with metal complexes. DNA binding study of the Cu-BIG complex shows hyperchromism due to the interaction of the complex with the base pairs of DNA[26] through non-covalent interactions, such as π–π stacking interactions, groove bindings, electrostatic interactions, hydrogen bonds and van der Waals interactions.[27] This is evident from the increase in the absorbance with an increase in the DNA concentration and these binding interactions of the complex with the CT-DNA have been studied with the help of absorption spectroscopy, emission spectroscopy and by viscosity measurements.

3.3a *Absorption spectroscopic studies*: The absorption spectrum of Cu-BIG complex was recorded by increasing the DNA concentration, which showed hyperchromism (Figure 4a). This is due to the interaction of the complex with DNA through van der Waals interactions. The magnitude of the hyperchromism depends on the extent of van der Waals interactions between DNA and the Cu-BIG Complex.

The concentration of CT-DNA was calculated from Beer's law and the ratio of absorbance at 260 and 280 nm is between 1.8 and 1.9, which indicates that the DNA is free from protein.[28] Absorption titration experiment was carried out with constant complex concentration (10 μM, cuvette pathlength, 10 mm) with varying DNA concentration (0–100 μM) in phosphate buffer. Solution of complex and DNA was incubated at 25°C for 10 min, after which absorbance readings were noted. The data was then fit into van Vleck equation[29] to obtain intrinsic binding constant, K_b:

$$[DNA]/[\varepsilon_a - \varepsilon_f] = [DNA]/[\varepsilon_b - \varepsilon_f] + 1/(K_b[\varepsilon_b - \varepsilon_f]) \quad (1)$$

where ε_a is the apparent extinction coefficient (A_obs/[DNA]) for each DNA + complex solution, ε_f is the extinction coefficient of the free complex and ε_b is the extinction coefficient of the fully bound complex with DNA. K_b is the intrinsic binding constant. The plot of $[DNA]/[\varepsilon_a - \varepsilon_f]$ versus [DNA] (Figure 4(b)) gave the intrinsic binding constant, K_b as a ratio of the slope to intercept. The K_b for Cu-BIG complex is $0.125 \times 10^5 M^{-1}$.

3.3b *Ethidium bromide fluorescence displacement experiments*: The apparent binding constants, K_{app} of Cu-BIG complex was calculated by using Stern–Volmer equation.[30] Fluorescence study of ethidium bromide (EtBr) bound CT DNA in the presence of a competing Cu-BIG complex in phosphate buffer (pH 7.2) was done at constant (10 μM) concentration of DNA by varying the complex concentration (10–500 μM). Each complex and DNA solution was incubated at 25°C for 10 min, after which emission spectra were recorded. Changes in emission intensity at 600 nm of EtBr bound to DNA were recorded with increasing amount of the Cu-BIGH complex concentration (Figure 5). In phosphate buffer (pH 7.2), EtBr was non-emissive due to fluorescence quenching of the free EtBr by the solvent molecules.[31,32] In the presence of DNA, EtBr showed enhanced emission intensity due to its intercalative binding to DNA. A

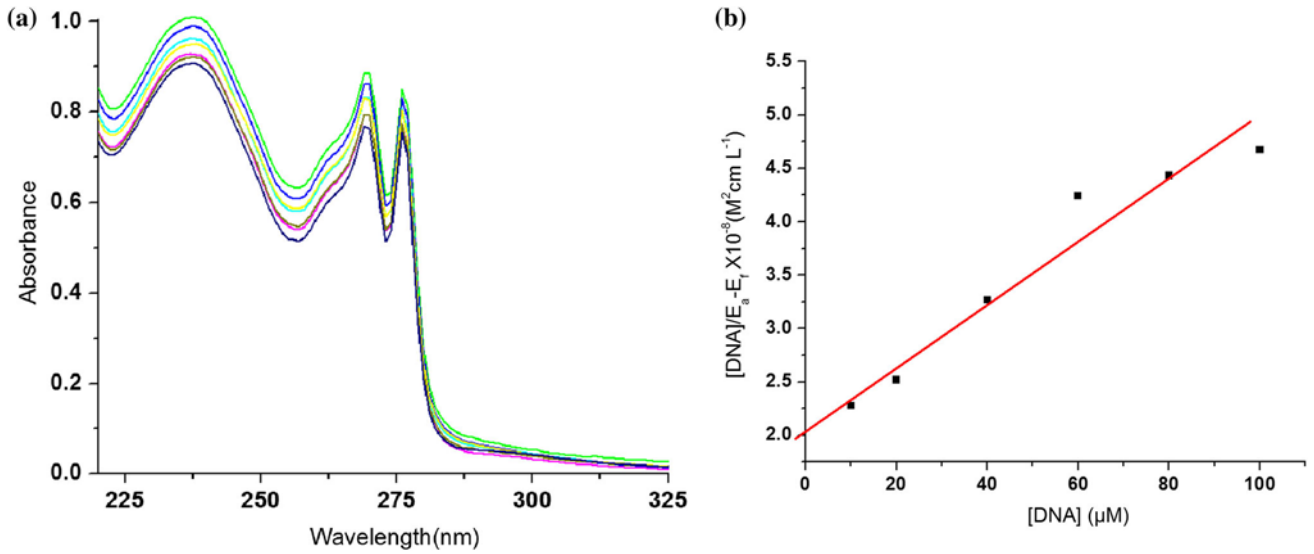

Figure 4. (**a**) Absorption spectra of Cu-BIG complex (50 μM, cuvette pathlength, 10 mm) for increasing concentration of DNA in phosphate buffer pH 7.0. (**b**) Plot of $[DNA]/[\varepsilon_a - \varepsilon_f]$ versus [DNA]. ($\varepsilon_f = 19968\ M^{-1}\ cm^{-1}$).

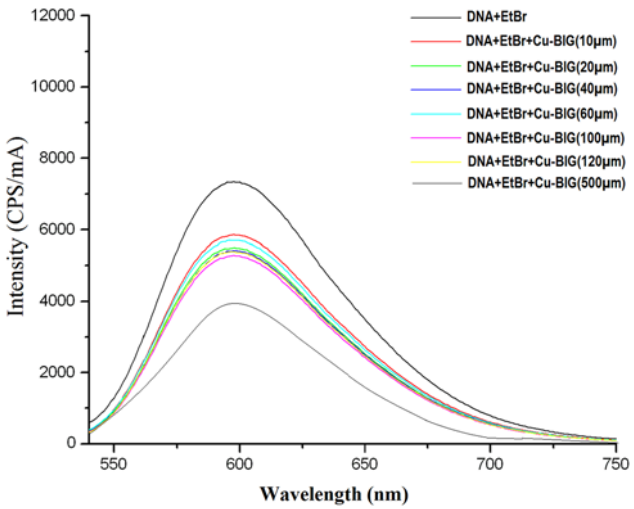

Figure 5. Emission spectra of Cu-BIG Complex, excited at 520 nm, for varying concentrations (10–500 μM).

competitive binding of the copper complex to CT DNA resulted in the displacement of the bound EtBr, decreasing its emission intensity. The apparent binding constant (K_{app}) was calculated from the following equation:[33]

$$K_{EtBr}\,[EtBr] = K_{app}\,[complex] \quad (2)$$

where K_{EtBr} is $1 \times 10^7\ M^{-1}$, EtBr concentration is 10 μM and [complex] is the concentration of the BIGH complex, for reduction of the emission intensity of EtBr by 50%. The K_{app} value for Cu-BIG is $2 \times 10^5\ M^{-1}$.

3.3c *Viscosity measurements*: Viscosity measurements were carried out using Oswald viscometer. Titrations were performed for Cu-BIG complex (20, 40, 60, 80, 100, 150 μL) solution (0.2 mM), which was introduced into the DNA solution (0.25 mM). Flow time was measured with a digital stopwatch, each sample was measured thrice and an average flow time was calculated and listed in Table S1 (Supplementary Information). Data was presented as $(\eta / \eta_0)^{1/3}$ versus the ratio of the concentration of Cu-BIG complex to DNA.[34] The DNA helixes lengthen as the base pairs are separated to accommodate the binding molecule, which leads to the increase of DNA viscosity. The plots of relative viscosities are shown in Figure S6 (Supplementary Information), which show an increase in the viscosity of the complex due to the binding of Cu-BIG with the DNA through intercalation. However, its binding ability is less when compared to classical intercalator like ethidium bromide.

$$(\eta/\eta_0)^{1/3} = \left[\left(\left(t_{complex} - t_0\right)/t_0\right) / \left(\left(t_{control} - t_0\right)/t_0\right)\right]^{1/3} \quad (3)$$

Here, $\eta = (t_{Complex} - t_0)/t_0$, $\eta_0 = (t_{Control} - t_0)/t_0$, $t_{Complex}$ = flow time of the complex for each titration (20, 40, 60, 80, 100, 150 μL), t_0 = flow time of the pure buffer (192 s) and $t_{control}$ = flow time of the CT DNA solution (211 s).

3.4 *Magnetic properties*

The magnetic properties of the polymeric complex, Cu-BIG have been studied using a vibrating sample magnetometer (VSM). The VSM spectrum (M–H) of magnetization (μ emu/g) versus magnetic field (G) was recorded. The M–H measurement area[35,36] and the curve

show that it is ferromagnetic in nature with low hysteresis loss. Variation of magnetization with applied field of Cu-BIG at 20 K and at room temperature are shown in the Figures 6 and 7, respectively, which show hysteresis loops of the compound measured by sweeping the external field between –1500 and 1500 G. The hysteresis loops are found to be extremely narrow. The squareness ratio for the particles is also extremely small. Narrow hysteresis loop implies that the compound is soft ferromagnetic and easier to magnetize and demagnetize in low fields. The corresponding parameters, saturation magnetization (Ms), retentivity and coercivity values obtained from the hysteresis loops are listed in Table 4. Low temperature measurements using VSM show that saturation magnetization increases with a decrease in temperature. The saturation magnetization at room tem-

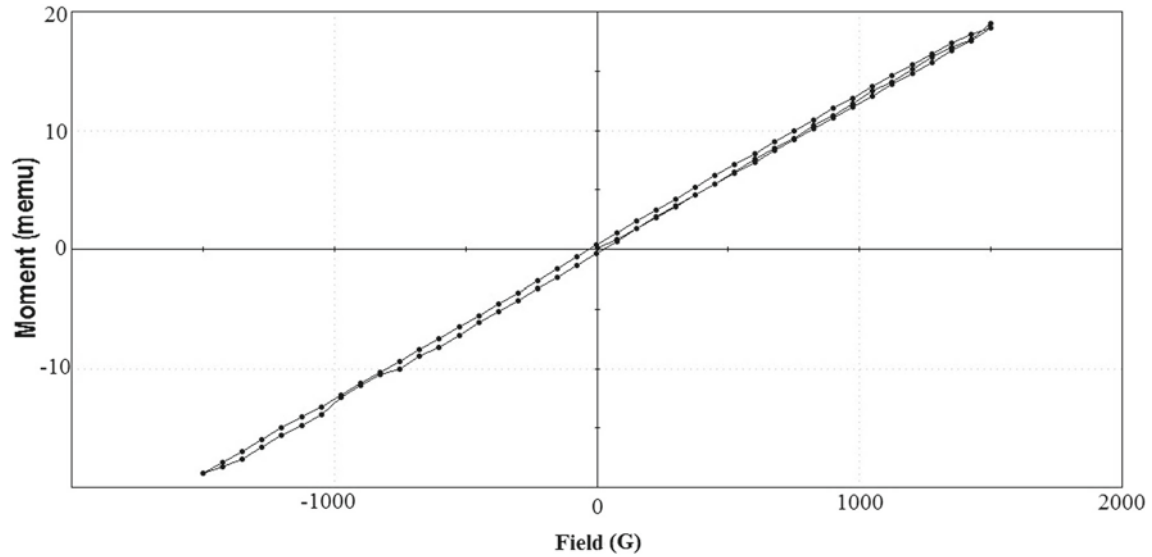

Figure 6. Variation of magnetization with applied field of Cu-BIG complex at 20 K.

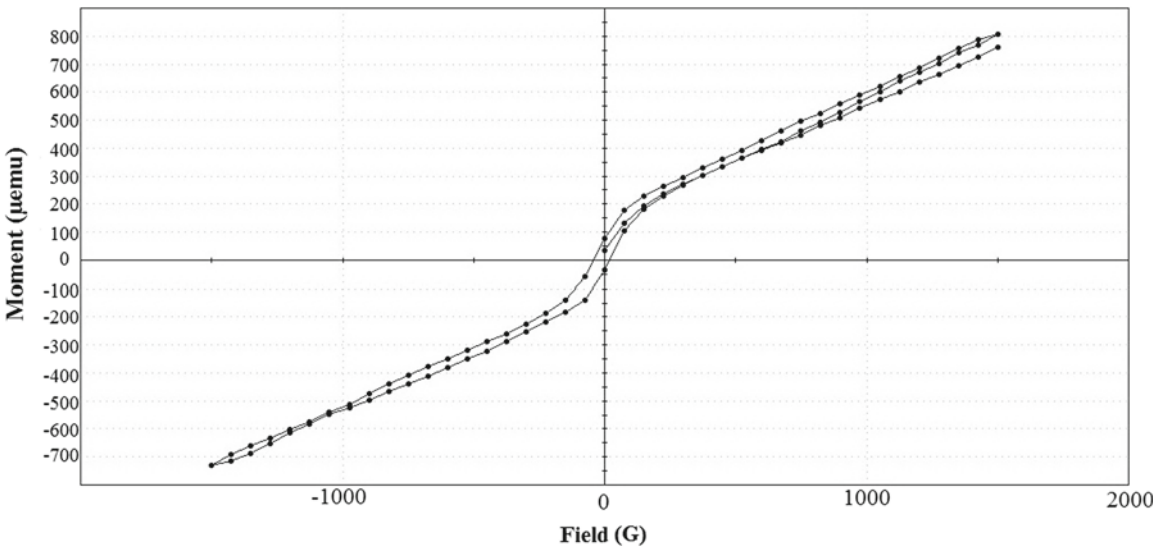

Figure 7. Variation of magnetization with applied field of Cu-BIG complex at room temperature.

Table 4. Magnetic data of Cu-BIG complex.

Temperature	Sat.Mag (Ms) emu/g	Coercivity (G)	Retentivity (Mr) emu/g	Squareness (Mr/Ms)
20 K	0.0189	265.15	0.365×10^{-3}	0.0193
Room temperature	0.769×10^{-3}	310.79	0.0571×10^{-3}	0.0743

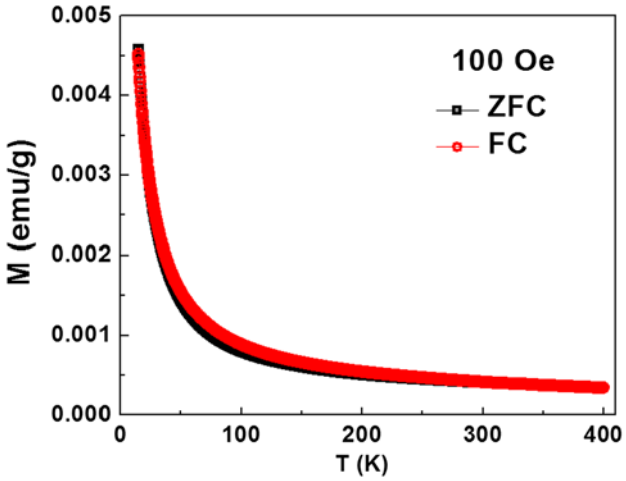

Figure 8. Magnetization versus temperature (M–T) plot of Cu-BIG (1) at H = 100 Oe.

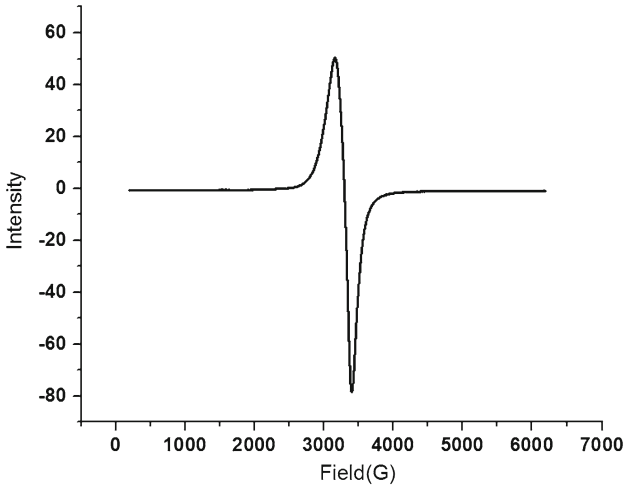

Figure 9. EPR spectrum of Cu-BIG complex.

perature is 0.769×10^{-3} emu/g, which increases to 0.0189 emu/g at 20 K and also shows an increase in coercivity with increase in temperature. As the temperature reaches the room temperature from 20 K, soft ferromagnetic nature shifts slowly to hard ferromagnetic due to an increase in hopping length.

The magnetization as a function of temperature and magnetic field of Cu-BIG (**1**) was studied using a superconducting quantum interference device (SQUID) magnetometer. Field-cooled (FC) and zero-field cooled (ZFC) magnetizations with temperature are shown in Figure 8.

Magnetic measurements of the compound were made at room temperature on a Gouy Balance. The effective magnetic moment (μ_{eff}) of **1** was found to be 2.088 BM. Magnetic moment of square planar Cu(II) complexes lies in the range of 1.70–1.90 BM.The higher value indicates distortion from square planar geometry,[37] which can be inferred from the crystal structure.

3.5 *EPR studies*

The EPR spectrum of the complex was recorded at room temperature and presented in Figure 9. EPR spectrum of the complex exhibits an isotropic spectrum with $g_{iso} = 2.121$.

3.6 *Electrochemical studies*

The redox properties of the complex were monitored by cyclic voltammetry. Cyclic voltammograms were recorded (Figures S7 and S8, in Supplementary Information) in aqueous solution with Ag/AgCl reference electrode at the potential range, −1.2 to +1.2 V in the presence of 0.1 M KCl as a supporting electrolyte.[38,39] The cyclic voltammogram of 1 M aqueous solution at 200 mV s^{-1} shows only one redox peak in the studied potential range, at +0.73 V for the oxidation in the forward scan and at +0.296 V for the reduction peak in the reverse scan. The peak potential separation, $\Delta E = (Epa - Epc)$, between the anodic and cathodic peaks is 434 mV. This large peak separation suggests that the reaction is quasi-reversible. The oxidation and reduction peak currents increase with the increase in scan rate. The effect of scan rate on the peak potential for the complex was also investigated by increasing the scan rate and the results are listed in Table S2 (Supplementary Information); the anodic peak potentials shift to more negative values and the cathodic peak potentials shift to more positive values. The increase in separation between the peak potentials, ΔE, by increasing the scan rate is a characteristic behaviour of a quasi-reversible system.

3.7 *Thermal analysis*

Thermal behaviour of the complex was studied by thermogravimetric analysis (TGA) and differential thermal analysis (DTA) recorded at 0–800°C, as shown in Figure 10. Thermogram of the complex shows only one stage of weight loss between 250 and 275°C which corresponds to the decomposition of the complex and the same is evident from the exothermic DTA curve. An initial endothermic peak in DTA curve at 59–65°C corresponds to phase transition of the compound, second endothermic peak at 110–120°C corresponds to the loss of coordinated water molecule.[40]

3.8 *Antibacterial activity*

In vitro antibacterial activities of BIGH and Cu-BIG were tested by the well-diffusion method under standard

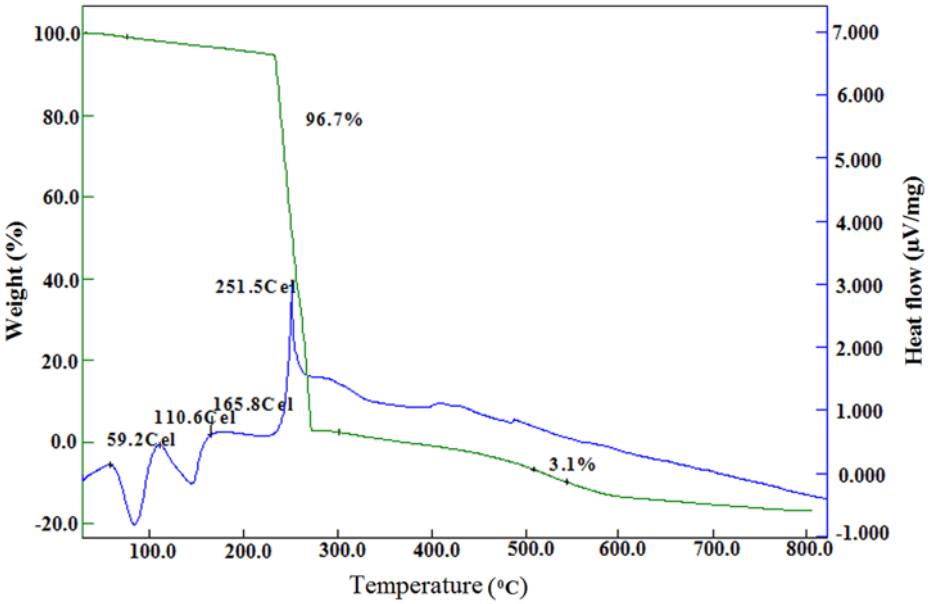

Figure 10. Thermogram of Cu-BIG complex.

conditions.[41] The strains chosen were G(+) *Staphylococcus aureus*, *Bacillus subtilis* and G(−)*Escherichia coli* and *Pseudomonas aeruginosa*. Bacterial subculture medium was autoclaved for 20 min before inoculation. Later, the bacteria were cultured for 24 h in an incubator at 37°C. Nutrient agar media plates were prepared and each plate was seeded with a pure test cultures by spread plate technique. Wells were bored into the media using a sterile tip and 20 μL of the test compounds ($\gamma = 1$ mg/mL) was inoculated into the well by micropipette. Then the plates were incubated at 37°C. The width of the growth inhibition zone was measured after 24 h of incubation. The results (Table S3 in SI) show that the Cu-BIG complex and BIGH are active against *Bacillus subtilis* and inactive against the other species. Further, the study evidently indicates that the antibacterial activity of the BIGH increased when coordinated to the Cu(II) ions. This is due to the greater lipophilic nature of the metal complex (Cu-BIG) than the free ligand (BIGH).

4. Conclusions

The Cu(II) coordination polymeric complex of benzimidazole-glycine conjugate ligand, Cu-BIG was synthesized under green conditions. Though there is no direct linkage between Cu–Cu in the polymeric complex, in Cu-BIG they are linked through carboxylate group of BIGH. The delocalized electron cloud of carboxylate group of BIGH induces indirect magnetic couple moments between copper ions, whereby it exhibits ferromagnetism. From the DNA binding studies, the apparent binding constant (K_{app}) and intrinsic binding constant (K_b) of Cu-BIG were found to be 2×10^5 M^{-1} and 0.125×10^5 M^{-1}, respectively. The cyclic voltammetric study shows that the Cu-BIG complex undergoes quasi-reversible reaction. The *in vitro* antibacterial activity study of Cu-BIG indicates that it is active against *Bacillus subtilis* with 2.9 cm zone of inhibition.

Supplementary Information (SI)

CCDC 1442822 contains the supplementary crystallographic data for this paper. This data can be obtained free of charge via http://www.ccdc.cam.ac.uk/conts/retrieving.html, or from the Cambridge Crystallographic Data Center, 12 Union Road, Cambridge CB2 1EZ, UK; Fax: (+44) 1223 336 033; or E-mail: deposit@ccdc.cam.ac.uk. The IR spectra of BIGH and Cu-BIG, NMR, CHNS of BIGH, UV spectrum of Cu-BIG, Relative viscosity of Cu-BIG, Cyclic voltammograms and Crystal structure with a clear view of coordinated water (Figures S1–S9) and viscosity data of Cu-BIG, Cyclic voltammetric data for Cu-BIG and at different scan rates and *in vitro* antimicrobial activity of BIGH and its copper complex (Tables S1–S3) are available in Supplementary Information at www.ias.ac.in/chemsci.

Acknowledgements

The authors are thankful to JNTU, Hyderabad and UGC networking resource centre, University of Hyderabad, India for providing necessary facilities to carry out this work.

References

1. Qin J H, Ma L F, Hu Y and Wang L Y 2012 Syntheses, structures and photoluminescence

of five zinc(II)coordination polymers based on 5-methoxyisophthalate and flexible N-donor ancillary ligands *CrystEngComm* **14** 2891
2. Yoon M, Srirambalaji R and Kim K 2012 Homochiral Metal–Organic Frameworks for Asymmetric Heterogeneous Catalysis *Chem. Rev.* **112** 1196
3. Moon H R, Lim D W and Suh M P 2013 Fabrication of metal nanoparticles in metal–organic frameworks *Chem. Soc. Rev.* **42** 1807
4. Gai Y L, Jiang F L, Xiong K C, Chen L, Yuan D Q, Zhang L J, Zhou K and Hong M C 2012 Temperature-Dependent in Situ Reduction of 4,4_-Azobispyridine via Solvothermal Reaction *Cryst. Growth Des.* **12** 2079
5. Vishnoi P, Kalita A C and Murugavel R 2014 An anionic two-dimensional indium carboxylate framework derived from a pseudo C_3-symmetric semi-flexible tricarboxylic acid *J. Chem. Sci.* **126** 1385
6. Tripathi S, Srirambalaji R, Singh N and Anantharaman G 2014 Chiral and achiral helical coordination polymers of zinc and cadmium from achiral 2,6-bis(imidazol-1-yl)pyridine: Solvent effect and spontaneous resolution *J. Chem. Sci.* **126** 1423
7. Janiak C 2003 Engineering coordination polymers towards applications *Dalton Trans.* **14** 2781
8. Rogez G, Viart N and Drillon M 2010 Multiferroic materials: the attractive approach of metal–organic frameworks (MOFs) *Angew. Chem. Int. Ed.* **49** 1921
9. Yu L, Wang Z, Wu J, Tu S and Ding K 2010 Directed Orthogonal Self-Assembly of Homochiral Coordination Polymers for Heterogeneous Enantioselective Hydrogenation *Angew. Chem. Int. Ed.* **49** 3627
10. Liu B, Zhao R L, Yang G P, Hou L, Wang Y Y and Shi Q Z 2013 Two isostructural amine- unctionalized 3D self-penetrating microporous MOFs exhibiting high sorption selectivity for CO *CrystEngComm* **15** 2057
11. Liu Y Y, Li J, Ma J F, Ma J C and Yang J 2012 A 2 series of 1D, 2D and 3D coordination polymers based on a 5-(benzonic-4-ylmethoxy)isophthalic acid: Syntheses, structures and photoluminescence *CrystEngComm* **14** 169
12. Suh M P, Park H J, Prasad T K and Lim D W 2012 Hydrogen Storage in Metal–Organic Frameworks *Chem. Rev.* **112** 782
13. Cui Y J, Yue Y F, Qian G D and Chen B L 2012 Luminescent Functional Metal–Organic Frameworks *Chem. Rev.* **112** 1126
14. Zhang H M, Yang J, Liu Y Y, Kang D W and Ma J F 2015 A family of coordination polymers assembled with a flexible hexacarboxylate ligand and auxiliary N-donor ligands: Syntheses, structures, and physical properties *CrystEngComm* **17** 3181
15. Fan L M, Zhang X T, Sun Z, Zhang W, Ding Y S, Fan W L, Sun L M, Zhao X and Lei H 2013 Ancillary Ligands Dependent Structural Diversity of A Series of Metal–Organic Frameworks Based on 3,5-Bis(3-carboxyphenyl)pyridine *Cryst. Growth Des.* **13** 2462
16. Lin L, Yu R M, Yang W B, Wu X Y and Lu C Z 2012 A Series of Chiral Metal–Organic Frameworks Basedon Oxalyl Retro-Peptides: Synthesis, Characterization, Dichroism Spectra, and Gas Adsorption *Cryst. Growth Des.* **12** 3304
17. Cheng P C, Kuo P T, Liao Y H, Xie M Y, Hsu W and Chen J D 2013 Ligand-Isomerism Controlled Structural Diversity of Zn(II) and Cd(II) Coordination Polymers from Mixed Dipyridyladipoamide and Benzenedicarboxylate Ligands *Cryst. Growth Des.* **13** 623
18. Liu S J, Xue L, Hu T L and Bu X H 2012 Two new CoII coordination polymers based on carboxylate-bridged di- and trinuclear clusters with a pyridinedicarboxylate ligand: Synthesis, structures and magnetism *Dalton. Trans.* **41** 6813
19. Verweij P D, van der Geest J S N, Driessen W L, Reedijk J, Sherrington D C 1992 Metal uptake by a novel benzimidazole ligand immobilised ontopoly(glycidyl methacrylate-co-ethylene glycol dimethacrylate *React. Polym.* **18** 191
20. SAINTPLUS Software for the CCD detector System 1998 *Bruker Analytical X-ray System Inc.* (Madidon, WI)
21. *SADABS* 1998 *Emperical Absorption Correction Program* (Madison, Wisconsin, USA: Bruker AXS Inc)
22. Sheldrick G M 1997 *Program for Crystal Structure Solution* (Germany: University of Gottingen)
23. Sheldrick G M 1997 *Program for Crystal Structure Refinement* (Germany: University of Gottingen)
24. Farrugia L J 1997 ORTEP-3 for Windows—a version of ORTEP-III with a Graphical User Interface (GUI) *J. Appl. Crystallogr.* **30** 565
25. Kepert D L 1982 *Inorganic Stereochemistry* (Berlin: Springer-Verlag) p. 65
26. Patra A, Sen S, Sarkar S, Zangrando E and Chattopadhyay P 2012 Syntheses, crystal structures, and DNA-binding of some nickel(II) complexes of 1,3-bis(2-pyridylmethylthio)propane and pseudohalides *J. Coord. Chem.* **65** 4096
27. Bimolini Devi A 2015 Synthesis, Characterization and DNA Interaction of Metal Complex of Nitrile group Ligand International *J. Basic Appl. Chem. Sci.* **5** 25
28. Reichman M E, Rice S A, Tgomas C A and Doty P 1954 A further examination of the molecular weight and size of desoxypentose nucleic acid *J. Am. Chem. Soc.* **76** 3047
29. Patra A, Sarkar S, Mukherjee T, Zangrando E and Chattopadhyay P 2011 Zinc(II) complexes of 1,3-bis(2-pyridylmethylthio)propane: Anion dependency, crystal structure and DNA binding study *Polyhedron* **30** 2783
30. Stern O and Volmer M 1919 The extinction period of fluorescence *Physik. Z.* **20** 183
31. Waring M J 1965 Complex formation between ethidium bromide and nucleic acids *J. Mol. Biol.* **13** 269
32. Changzheng I. Jigui W, Liufang W, Min R, Naiyang J and Jie G 1999 Synthesis, characterization and antitumor activity of copper(II) complex with nicotinamido-4-bis(2-chloroethyl)aminobenzaldimine *J. Inorg. Biochem.* **73** 195
33. Lee M, Rhodes A L, Wyatt M D, Forrow S and Hartley J A 1993 GC base sequence recognition by oligo(imidazolecarboxamide) and C-terminus-modified analogues of distamycin deduced from circular dichroism, proton nuclear magnetic resonance, and methidiumpropylethylenediaminetetraacetate-iron(II) footprinting studies *Biochemistry* **32** 4237
34. Zhi B O, Yu Hao L, Yan Mei L, Shi Chen, Ya Hong X and Xiao Hua Z 2013 A copper(II) complex with

2-(2′-pyridyl)benzimidazole and l-arginine: synthesis, structure, antibacterial activities, and DNA interaction *J. Coord. Chem.* **66** 2152

35. Valeska da R C and Tsuneharu O 2003 Microstructure and Hysteresis Curves of Samarium-Holmium-Iron Garnet Synthesized by Coprecipitation *Mat. Res.* **6** 569
36. Chao L, Rondinone A J and Zhang Z J 2000 Synthesis of magnetic spinel ferrite $CoFe_2O_4$ nanoparticles from ferric salt and characterization of the size-dependent superparamagnetic properties *Pure Appl. Chem.* **72** 37
37. Raziyeh A A and Saeid A 2012 Synthesis, Spectroscopy, Thermal Analysis, Magnetic Properties and Biological Activity Studies of Cu(II) and Co(II) Complexes with Schiff Base Dye Ligands *Molecules* **17** 6434
38. Rong-kai P, Guo-bi Li, Sheng-gui Liu, Xiao-ping Z and Gui-zhen Y 2016 Synthesis, crystal structure, electrochemical property, and antioxidant activity of copper(II) complex based on 4-butyloxy-2,6-bis(1-methyl-2-benzimidazolyl)pyridine *Monatsh. Chem.* **147** 1189
39. Mohamed M I, Gaber A M M, Samir A E S and Abdel-Motaleb M R 2012 Synthesis, Characterization, and Electrochemical Properties of Bis(2-benzimidazolylmethyl-6-sulfonate)amine-based zinc(II), copper(II), and oxidovanadium(IV) Complexes: SOD Scavenging, DNA binding, and Anticancer Activities *Int. J. Electrochem. Sci.* **7** 7526
40. Kavi Rasu K, Balaji D and Moorthy Babu S 2016 Spectroscopic properties of Eu^{3+} : $KLa(WO_4)_2$ novel red phosphors *J. Lumin.* **170** 547
41. Souza S M, Delle–Monache F and Smânia Jr A 2005 Antibacterial Activity of Coumarins *Z. Naturforsch. C* **60** 693